

- Technology of Electroceramic Thin Films*, O. Auciello and R. Waser, Eds. (Kluwer Academic, Dordrecht, Netherlands, 1995), pp. 1–22.
21. The committee is chaired by H. Koinuma, Tokyo Institute of Technology.
 22. S. Jin *et al.*, *Science* **264**, 413 (1994).
 23. S. Jin *et al.*, *Appl. Phys. Lett.* **67**, 557 (1995).
 24. E. E. Fullerton *et al.*, *ibid.* **63**, 1699 (1993).
 25. D. R. McKenzie, D. Muller, B. A. Pailthorpe, *Phys. Rev. Lett.* **67**, 773 (1991).
 26. S. D. Berger, D. R. McKenzie, P. J. Martin, *Philos. Mag. Lett.* **57**, 285 (1988).
 27. F. Davanloo, E. M. Juengerman, D. R. Jander, T. J. Lee, C. B. Collins, *J. Appl. Phys.* **67**, 2081 (1990); C. B. Collins *et al.*, *ibid.* **69**, 7862 (1991); F. Davanloo *et al.*, *ibid.* **71**, 1446 (1992); C. B. Collins, F. Davanloo, T. J. Lee, H. Park, J. H. You, *J. Vac. Sci. Technol. B* **11**, 1936 (1993).
 28. J. J. Cuomo, D. L. Pappas, J. Bruley, J. P. Doyle, K. L. Saenger, *Appl. Phys.* **70**, 1706 (1991).
 29. D. L. Pappas *et al.*, *ibid.* **71**, 5675 (1992); D. L. Pappas, K. L. Saenger, J. J. Cuomo, R. W. Dreyfus, *ibid.* **72**, 3966 (1992).
 30. F. Xiong, Y. Y. Wang, V. Leppert, R. P. H. Chang, *J. Mater. Res.* **8**, 2265 (1993); F. Xiong, Y. Y. Wang, R. P. H. Chang, *Phys. Rev. B* **48**, 8016 (1993).
 31. A. A. Puzos, D. B. Geohegan, G. E. Jellison Jr., M. McGibbon, in *Film Synthesis and Growth Using Energetic Beams*, H. A. Atwater, J. T. Dickinson, D. H. Lowndes, A. Polman, Eds. (Materials Research Society, Pittsburgh, PA, 1995), vol. 388, pp. 145–150; *Appl. Surf. Sci.* **96–98**, 859 (1996).
 32. N. A. Marks, D. R. McKenzie, B. A. Pailthorpe, M. Bernasconi, M. Parrinello, *Phys. Rev. Lett.* **76**, 768 (1996).
 33. See the recent review by J. E. Jaskie, *Mater. Res. Soc. Bull.* **21**, 59 (1996).
 34. An intensified charge-coupled device (CCD)-array camera system coupled to a tunable (400 to 720 nm) narrow-band (full width at half maximum, 5 nm) liquid-crystal filter was used for species-resolved spectroscopic imaging. The ability to study simultaneously both fast- and slow-moving components of the ablation plume results from the extreme (photon counting) sensitivity of the intensified CCD-array camera system and its ability to collect photons from all wavelengths simultaneously. Slow-moving or scattered components of the laser-sputtered flux (such as redeposited material near the target) are not overlooked. For details and other examples of gated, species-resolved imaging, see (4) and D. B. Geohegan and A. A. Puzos, *Mater. Res. Soc. Symp. Proc.*, in press.
 35. D. Feiler, R. S. Williams, A. A. Talin, H. Yoon, M. S. Goorsky, *J. Cryst. Growth*, in press.
 36. C. M. Rouleau *et al.*, *Appl. Phys. Lett.* **67**, 2545 (1995).
 37. D. H. Lowndes *et al.*, *Mater. Res. Soc. Symp. Proc.*, in press.
 38. C. M. Rouleau *et al.*, *ibid.*, in press.
 39. Time-resolved ion current measurements during the ablation of various materials have revealed that over a limited range of ambient gas pressures, the ablation plume generally splits into two or more components that travel at different average velocities and KEs. For a detailed description of ion current measurements and the “plume splitting” phenomenon, see (4) and also D. B. Geohegan and A. A. Puzos, *Appl. Phys. Lett.* **67**, 197 (1995); *Appl. Surf. Sci.* **96–98**, 131 (1996).
 40. K.-D. Rinnen, K. D. Kolenbrander, A. M. DeSantolo, M. L. Mandich, *J. Chem. Phys.* **96**, 4088 (1992).
 41. L. A. Chiu, A. A. Seraphin, K. D. Kolenbrander, *J. Electron. Mater.* **23**, 347 (1994).
 42. Similar pulsed laser ablation supersonic expansion sources were first developed by Smalley and co-workers nearly 15 years ago [D. E. Powers *et al.*, *J. Phys. Chem.* **86**, 2556 (1982)].
 43. T. Yoshida, S. Takeyama, Y. Yamada, K. Mutoh, *Appl. Phys. Lett.* **68**, 1772 (1996).
 44. See L. Canham, *Mater. Res. Soc. Bull.* **18**, 22 (1993).
 45. W. M. K. P. Wijekoon, M. Y. M. Lykley, P. N. Prasad, J. F. Garvey, *Appl. Phys. Lett.* **67**, 1698 (1995).
 46. This research was carried out at Oak Ridge National Laboratory (ORNL), managed by Lockheed Martin Energy Research Corporation for the U.S. Department of Energy under contract DE-AC05-96OR22464. C.M.R. was supported by an appointment to the ORNL Postdoctoral Research Associates Program administered jointly by ORNL and the Oak Ridge Institute for Science and Education.

Chemical Solution Routes to Single-Crystal Thin Films

F. F. Lange

Epitaxial thin films of inorganic single crystals can be grown on single-crystal substrates with a variety of different solution chemistries. This review emphasizes chemical solution deposition, in which a solution is used to deposit a layer of precursor molecules that decompose to low-density, polycrystalline films during heating. Ways to control film cracking during deposition and heat treatment and why many precursors synthesize metastable crystalline structures are discussed, and the different mechanisms that convert the polycrystalline film into a single crystal are reviewed. Hydrothermal epitaxy, in which single crystal thin films are directly synthesized on templating substrates in an aqueous solution at temperatures <150°C, is also discussed.

Inorganic, single-crystal thin films can be produced from solution (either aqueous or organic) that contain precursor molecules for the different elements in the multielement compound of interest. Solution routes are relatively new and have been explored for possible device applications (such as nonvolatile memories, pyroelectric detectors, and field-emission displays) as an alternative to more costly vapor-phase routes (1). Oxide compositions, specifically those with unusual electro-optical properties, such as LiNbO₃ (2, 3) and Pb(Zr,Ti)O₃ (4, 5), and others including rare-earth aluminates (6), cuprate superconductors (7, 8), and other oxides (9–14), have received most of the attention. Growth of single-

crystal carbides (15), nitrides, and a limited group of metals is possible. As in the many different vapor-phase routes (1), single-crystal substrates are used as a supporting structure and a template for the oriented overgrowth of the film material—a process known as epitaxy.

The chemical solution deposition route to epitaxial films has received the most technical attention and will be the focus of this review. In this route, the solution is merely a vehicle to deposit, either by spin-coating or dip-coating, the desired elements onto a single-crystal substrate. A solid precursor film forms that decomposes (pyrolyzes) to a polycrystalline inorganic film during heating. The polycrystalline film converts to a single-crystal film at higher temperatures by one of a number of mechanisms described below. A number of dif-

ferent phenomena effect epitaxy. Different solution precursor chemistries can be used to produce the same inorganic material. The different precursor coatings can have different properties that include different rheological behaviors that influence coating coverage, different mechanical properties that affect cracking during processing, and different decomposition products that can alter the composition formed during pyrolysis. The large volume decrease produced during evaporation and pyrolysis will lead to the formation of “mud” cracks if the film thickness is greater than a critical value. Because the inorganic material is formed by pyrolysis at temperatures where diffusion is kinetically limited, metastable phases can crystallize to effect epitaxy during their transformation to the stable phase. In addition to these subjects, the effect of differences in crystal structure between the film and substrate on the epitaxy phenomena will also be reviewed.

In a second route, hydrothermal epitaxy, the single-crystal thin film is directly synthesized on a substrate in water at temperatures ≤150°C. This route only warrants a few paragraphs because it has just “seen the light of literature.”

One advantage of solution routes is the economics that “beakers and benches” chemistry offer relative to capital-intensive vapor-phase routes. A second is the high degree of compositional control inherent with the solution synthesis of multielement, inorganic materials. Also, the newly introduced hydrothermal route offers processing temperatures that approach ambient conditions, which would be very advantageous for sequential processing of devices where

The author is in the Materials Department, University of California, Santa Barbara, CA 93106, USA.

interdiffusion of previously processed components must be avoided. The apparent disadvantage of the solution routes is the lack of understanding relating processing, film quality, and properties. For example, with certain vapor-phase routes (1), mass is added atom-by-atom and the single-crystal film grows by mechanisms that depend on the lattice mismatch strain between the film and substrate. These mechanisms include atomic layer-by-layer growth and growth by island nucleation and coalescence. The range of defects introduced by these growth mechanisms have been studied for vapor-phase routes (1), whereas these relations are just being uncovered for solution routes. Because this approach is so new, it will be obvious to some readers, especially chemists who find new opportunities hidden in every beaker, that both minor changes and major perturbations will lead to innovations.

Precursor Chemistries

A variety of precursor chemicals that include metal organic molecules (16–21), metal salts (22), and polymers (23) can be pyrolyzed to synthesize oxides, carbides, nitrides and certain metals at modest temperatures (usually between 150° and 500°C). Multielement compounds can be synthesized by mixing similar precursor molecules in a common solvent prior to pyrolysis. An example is the cuprate superconductor, $\text{Bi}_{2.1}\text{Sr}_{1.6}\text{Ca}_{0.9}\text{Cu}_2\text{O}_x$, synthesized by mixing bismuth, strontium, calcium, and copper 2-ethyl-hexanoates, each assayed for their specific metal oxide, in toluene (8). 2-Ethyl-hexanoates, emphasized by Vest and co-workers (19, 20) for the processing of polycrystalline oxide films, are a specific metal carboxylate, where n in Fig. 1A is the valance of the metal ion and R is a specific branched hydrocarbon chain. These precursors cleanly pyrolyze to metal oxides and

gaseous hydrocarbons, even in inert atmospheres. Metal acetates ($\text{R} = \text{CH}_3$) are another type of carboxylate with a much smaller hydrocarbon chain that allows them to dissolve in water. Some, like zirconium acetate, do not cleanly pyrolyze, but produce residual carbon, which must be removed by oxidation, as well as ZrO_2 (21).

Although metal carboxylates, such as 2-ethyl-hexanoates, do not bond together when mixed, other molecules like metal alkoxides (Fig. 1A) react together when water is added to their common solvent to form a "double-alkoxide" precursor molecule with a specific cation/cation ratio. The one shown in Fig. 1B can be used to synthesize the ferroelectric material BaTiO_3 (17). "Hybrid" alkoxide precursor molecules (Fig. 1C) can be produced (24) with a specific cation ratio, for example, by reacting anhydrous lead acetate with titanium alkoxide in a common solvent. It is a widely used precursor for the pyroelectric material, PbTiO_3 . Precursors for PZT [ferroelectric compositions within the solid-solution series, $\text{Pb}(\text{Zr,Ti})\text{O}_3$] can be formulated by mixing, the two hybridized precursors, $\text{AcPbOZr}(\text{OR})_3$ and $\text{AcPbOTi}(\text{OR})_3$ (Ac, acetyl) (25).

The great popularity of alkoxide precursors stems from their ability to form polymeric species composed of metal-oxygen-metal (M–O–M) bonds when reacted with water (16, 17). Two reactions, one where a water molecule partially hydrolyzes the alkoxide molecule (Fig. 1D), and a second where a partially hydrolyzed molecule reacts with another alkoxide molecule (Fig. 1E), are needed to form the M–O–M network. The viscosity of the solution increases with the molecular weight of the reacted species. When concentrated by evaporation, the polymeric species form a gel composed of the three-dimensional M–O–M network (17) within the alcohol, with a substantial fraction of terminating, unreacted –M–OH and –M–OR groups. Unlike precursor solutions con-

taining mixed 2-ethyl-hexanoates that evaporate to form soft, "soapy" substances, alkoxide solutions, which are either purposely pre-reacted with water or allowed to react with atmospheric water, form brittle gels.

Many other precursors form gels. "Aluminum oxychloride," an aqueous solution of AlCl_3 containing partially hydrolyzed Al^{3+} ions at pH 5, forms a gel when concentrated during evaporation (22). Likewise, zirconium acetate species in aqueous solution also gel when concentrated (21). Other precursors form "solid" resins when complexing agents are introduced to cross-link specific species.

Figure 2 shows the loss of weight for two different precursors; both pyrolyze to $\text{Pb}(\text{Zr}_{0.5}\text{Ti}_{0.5})\text{O}_3$, a useful ferroelectric material (26). Relative to the hydrolyzed hybrid alkoxide, the mixed 2-ethyl-hexanoate precursor exhibits a large weight loss because of its much larger hydrocarbon content. In this case, the large volume of gaseous hydrocarbons produced during the pyrolysis cause Pb to separate from the other elements because it forms a Pb vapor at the pyrolysis temperature instead of forming an oxide.

As pointed out by Mantese *et al.* (20), metal carboxylates can directly produce certain metals, including Pb, Bi, Sn, and Cu, because they can cleanly pyrolyzed within a "window" of oxygen partial pressure where the metal, instead of its oxide, is thermodynamically stable. Noble metals, such as Ag, Au, and Pt, can also be formed by the pyrolysis of carboxylate precursors; these "resin" precursors are commonly used as "inks" to produce decorative coatings on up-market products.

Avoiding Mud Cracks

Solutions precursors are used to form a solid, precursor film on a substrate by either spin-coating (27) or dip-coating (17). The technologies for producing coatings with a uniform thickness over large areas via spin-coating have been well developed in the electronic industry where photoresist coatings

Fig. 1. (A) Metal carboxylate molecule (top) and metal alkoxide molecule (bottom). (B) Double-alkoxide molecule. (C) Hybrid alkoxide molecule. (D) Partial hydrolysis of a metal-alkoxide molecule. (E) Formation of a –M–O–M– bond toward the formation of an oxide gel.

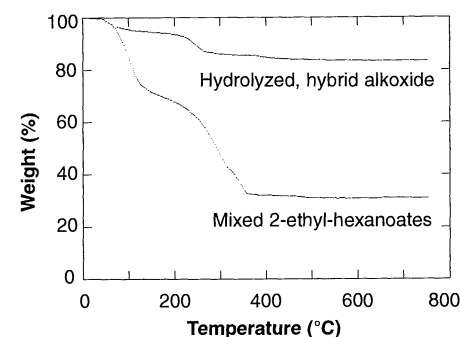
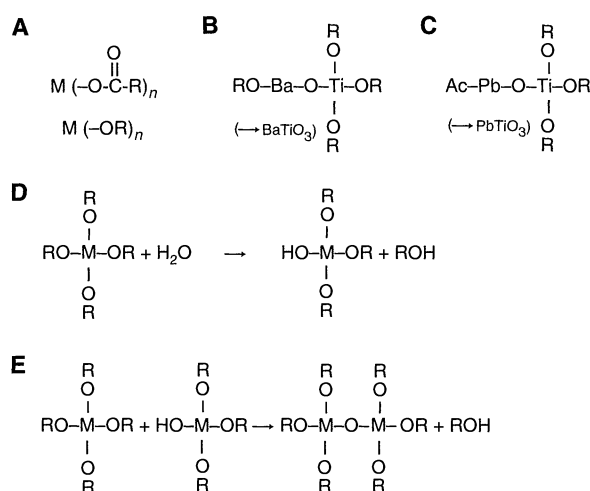


Fig. 2. Thermogravimetric analysis of two precursors used to synthesize $\text{Pb}(\text{Zr}_{0.5}\text{Ti}_{0.5})\text{O}_3$, dried prior to analysis.

are commonly used to make patterns, and in the glass industry where SnO₂ antireflective coatings are produced by dip-coating large sheets of glass with an alkoxide precursor (31). During coating, the excess solvent evaporates to produce a solid precursor film with mechanical properties that depend on the precursor, for example, soapy for some surfactant precursors like the hexanoates, and brittle for gel-forming precursors.

The pyrolyzed inorganic material is very porous because a large fraction of the precursor volume is eliminated during pyrolysis as volatile hydrocarbon gases, or water vapor, or both. Immediately after crystallization, the microstructure of the inorganic substance is an irregular, porous array of very small (~2 nm) crystallites that are chemically bonded to one another, much like a partially dense compacted powder. Further heating is required to cause the material to become fully dense through the usual mass-transport phenomena associated with densification.

Because the film significantly decreases its volume during evaporation, pyrolysis, and densification, biaxial tensile stresses arise within the film because the shrinkage is constrained by the substrate. These tensile stresses can be relieved by the propagation of cracks that form a mud crack pattern. Such cracks can be avoided if the film is produced with a thickness that is less than a critical value. For many precursors that produce brittle gels, the critical thickness is ~100 nm.

The reason for a critical thickness can be understood with the help of Fig. 3, which shows a thin film with a small crack of length *c* that is assumed to penetrate the film thickness *t*. The film is assumed to be an elastic material with a Young's modulus *E* and a Poisson's ratio *ν* and subjected to a biaxial tensile stress *σ*. Because the tensile force within the film times the cross-sectional area of the film must be equal to the compressive force within the substrate times the cross-sectional area of the substrate, the compressive stresses within the substrate can be neglected when the film is very thin relative to the substrate. That is, only the tensile stress within the film need be considered. The strain energy stored in the film, per unit volume is $\sigma^2(1 - \nu)/(2E) = \sigma^2/2E^*$. The strain energy within the film containing the small crack is $U_{se}^0 -$

$[\sigma^2/2E^*]Zct^2$, where U_{se}^0 is the initial strain energy within the uncracked film and Zct^2 is the volume of material around the crack where strain energy is relieved. The energy needed to form the crack's surface is ctG_c , where G_c is the energy needed to form two crack surfaces per unit area (G_c is also known in the fracture mechanics literature as the critical strain-energy release rate), and ct is the area of the crack. Neglecting the internal energy, the total energy associated with the cracked film is:

$$U_t = U_{se}^0 - [\sigma^2/(2E^*)]Zct^2 + G_c ct \quad (1)$$

To find the conditions where the crack will extend along the film, we apply the concept introduced by A. A. Griffith more than 70 years ago. That is, a crack can only extend if it reduces the free energy of the system, that is, if $\partial U_t/\partial c \leq 0$. Differentiating Eq. 1 with respect to *c*, one finds that the condition for crack extension does not depend on the length of the crack, but instead, depends on the film thickness:

$$\frac{\partial U_t}{\partial c} \leq G_c t - Z[\sigma^2/(2E^*)]t^2 \quad (2)$$

Setting Eq. 2 equal to zero, one can now understand why a crack cannot extend until the film thickness exceeds a critical value:

$$t \geq t_c = 2G_c E^*/(Z\sigma^2) \quad (3)$$

More rigorous analyses (28, 29) for a variety of different crack geometries, such as cracks that not only extend across the film but concurrently extend either along the interface or into the substrate, leads to the same conclusion. The value for the dimensionless parameter *Z* differs for each type of crack (29), but the conclusion is the same, namely, crack extension can be avoided provided the film thickness does not exceed a critical value.

Optimizing the conditions that avoid cracking has been limited to producing precursor films with a thickness to less than the critical value. Processors have learned to form thicker films by building up the film thickness with cyclic coating and pyrolysis steps, thus avoiding cracking during each cycle. This cyclic coating procedure is expected to introduce defects. Observations suggest that brittle precursors (gels) form their mud crack pattern during drying when G_c apparently has its lowest value. Also, brittle gels are more prone to cracking than

soapy carboxylate films, suggesting that research directed to increase the G_c of the dried precursor would be fruitful.

Crystallization and Metastable Phases

Crystallization of the inorganic compound is usually concurrent with pyrolysis (30). When the composition is far from the equilibrium composition, crystallization can be delayed to much higher temperatures (31). Because pyrolysis occurs at very low temperatures relative to the compound's melting temperature, the free energy change for crystallization is large, and the critical nucleus size required for spontaneous crystallization is very small. Thus, the crystallization of a connective (partially sintered) network of nanocrystallites (<2 nm) is observed. In addition, because crystallization occurs at low temperatures, where diffusion is kinetically limited, metastable phases (extended solid-solutions and nonequilibrium structures) can crystallize (30, 31).

The concept of kinetically limited crystallization can be illustrated with the help of Fig. 4, which schematically shows free energy functions of three stable phases and three metastable phases as a function of composition for the PbO-TiO₂ binary system at ~400°C, where crystallization is first observed after pyrolysis (25). The three equilibrium phases are PbO, TiO₂, and PbTiO₃ (perovskite structure) with specific compositions located in the binary by the minimum for their respective free energy functions. The three metastable phases are the amorphous oxide produced during pyrolysis (upper line that spans the binary), the pyrochlore structure, and the compound, PbTi₃O₇. When a Ti-rich composition (*x*) is formulated by mixing Ti- and Pb-precursors [such as the hybrid alkoxide,

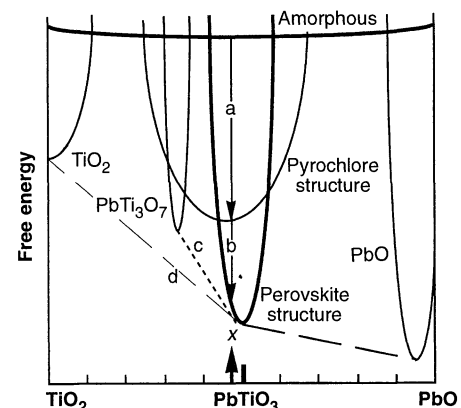
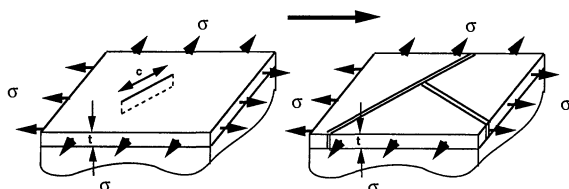


Fig. 4. Schematic of the free energy versus composition functions for phases found in the PbO-TiO₂ binary system at a temperature within the range of 400° to 800°C (25).

Fig. 3. Portion of a thin film bonded to a thicker substrate containing a crack of length *c*, which extends (right hand view) along the length of the film to form a mud crack pattern with the extension of other cracks.



AcPbOTi(OR)₃ plus Ti(OR)₄, or Pb- and Ti- hexanoates) and pyrolyzed at ~400°C, it produces an amorphous oxide (25). At slightly higher temperatures, the amorphous phase crystallizes as a single phase, with the pyrochlore structure as shown by the arrow a in Fig. 4. It is believed that the composition that crystallizes first has the pyrochlore structure, instead of the lower free energy perovskite structure, because pyrochlore offers greater freedom for placement of Pb and Ti ions on cation sites and offers the greater possibility of vacancies on oxygen sites. That is, at temperatures where diffusion is severely limited, the pyrochlore structure is kinetically more favorable. When heated to higher temperatures, the metastable pyrochlore structure transforms to the perovskite structure as shown by the arrow b, but retains its metastable, Ti-rich composition. At still higher temperatures, the metastable perovskite partitions into two phases: a metastable Ti-rich phase (PbTi₃O₇) and a perovskite phase with a composition that approaches the stoichiometric equilibrium phase, PbTiO₃ as shown by the dashed line c. At still higher temperatures, the system

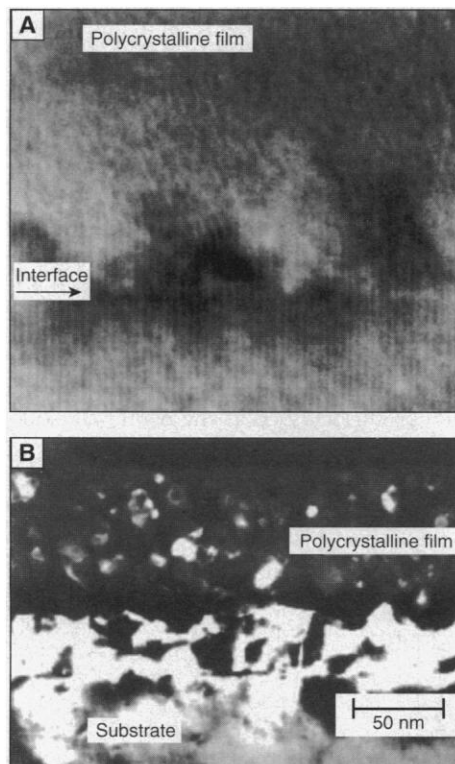


Fig. 5. (A) A cross-sectional view of a polycrystalline Zr(Y)O₂ film formed on a (100) cubic-Zr(Y)O₂ single-crystal substrate grains at the substrate interface that have nucleated with the same orientation during pyrolysis (distance between lattice fringes is ~2.5 nm) and (B) dark-field TEM of the same film heat treated at 900°C showing partial conversion of the polycrystalline film to a single crystal by grain growth (11).

reacts to finally form the two stable phases, TiO₂ (rutile) and PbTiO₃ (perovskite) as shown by the dashed line d. Each of these kinetically limited steps (a → d) sequentially decreases the free energy.

The phenomena of diffusion-limited crystallization is commonly observed in many different materials produced from precursors because they are synthesized in the solid-state at very low temperatures. Examples for single oxides are the crystallization of Al₂O₃ with the metastable γ structure instead of the stable α structure and the crystallization of TiO₂ as anatase instead of the stable rutile structure. As shown below, these metastable phases effect epitaxy.

Epitaxial Grain Growth

A number of different phenomena can convert the polycrystalline film formed during pyrolysis into a single crystal. When the film and substrate have identical structures, despite different chemistries, and their lattice mismatch is small, the epitaxy phenomenon simply involves the growth of nanometer epitaxial grains located at the film/substrate interface (Fig. 5A) that are produced during pyrolysis (22). The darker grains at the interface have lattice fringes that extend from the substrate. Miller *et al.* (11) uncovered this growth mechanism during studies where aqueous solutions of zirconium acetate and yttrium nitrate were used to coat (100) cubic-Zr(Y)O₂ (9.5 mol% Y₂O₃) substrates. Film compositions within the range cubic-Zr(Y)O₂ (6 to 40 mol% Y₂O₃) had a lattice mismatch up to 1.59%. Miller *et al.* showed that although the nanometer epitaxial grains are produced at the film/substrate interface during pyrolysis (~400°C), higher temperatures were needed to sufficiently densify the film to allow the epitaxial grains to grow to the surface by consuming the other misoriented grains. The elimination of grain boundaries in the initial polycrystalline film is the apparent free energy driving the epitaxial grain growth phenomenon.

A dark-field transmission electron microscopy (TEM) image (Fig. 5B) shows that

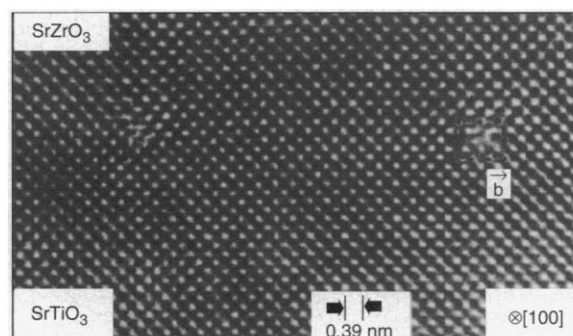
a 900°C, the epitaxial layer (mismatch = 0.81%) has grown approximately half-way to the surface within the polycrystalline film. Most of the epitaxial film and substrate are brighter because the image is taken with a common diffraction beam from the substrate and epitaxial film. Grains that have a small misorientation were not consumed during epitaxial grain growth and appear as darker, defect "grains." Higher temperatures (~1100°C) were needed to fully grow the film to the surface and to eliminate many of the internal defects observed at lower temperatures. At 1100°C, the surface was not smooth but contained pits caused by the remnant pores "pushed" to surface by the moving epitaxial front. Surface diffusion produced smooth surfaces at higher temperatures (>1200°C).

When the film and substrate had nearly the same composition and thus nearly no mismatch strain, the epitaxial grain growth phenomenon initiated at a lower temperature relative to compositions with a larger mismatch. For this case, pores within the partially dense, polycrystalline film would become internally trapped as it was converted into a single-crystal film. Trapped pores were difficult to remove by heat treatment because of the lack of intersecting grain boundaries, which are rapid paths for mass transport (10). The strain energy associated with the initial epitaxial growth may help retard growth until higher temperatures are reached, when pores can move with the epitaxial front (11).

The same study (11) showed that much of the strain energy within the film due to the lattice mismatch was relieved by the formation of a dislocation network at the film/substrate interface as observed for vapor grown films (1, 32). To a first approximation, the interfacial energy might be estimated to be solely due to the dislocation network. For atomic layer-by-layer growth in vapor-phase epitaxy, it is believed that the dislocations move from the surface to the interface (1). How the dislocation network forms at the interface is still unknown for the solution deposition route.

To understand how the epitaxy mecha-

Fig. 6. Cross-sectional view, (100) zone axis, of an interface between epitaxial SrZrO₃ film and (001) SrTiO₃ substrate, showing periodic missing planes in SrZrO₃ crystal that compensates for much of the lattice mismatch strain due to the larger (5%) lattice parameter of the SrZrO₃. Note the Burgers circuit around the dislocation at the interface (13).



nism might change with lattice mismatch, two studies are currently under way. One involves the epitaxy of metal oxides (CdO, CaO, and SrO) on MgO; all have the NaCl structure with lattice mismatch between 11 and 23% (33). The second involves a series of solid-solution compositions, (Sr,Ba)-(Ti,Zr,Ce)O₃, grown on either SrTiO₃ or LaAlO₃ (13), with a lattice mismatch between 0 to 16%; in this series both films and substrates have the perovskite structure. In both studies, 2-ethyl-hexanoate/toluene are the precursor solutions. Figure 6 shows the closely spaced and periodic dislocations at the SrZrO₃/SrTiO₃ interface (13). The dislocation spacing s is nearly identical to that predicted with the relation $s = b/\epsilon$, where b is the Burger's vector of the dislocation and ϵ is the strain associated with the lattice mismatch (32). Because the film has a larger lattice parameter relative to the substrate, the edge dislocations that terminate at the interface are missing planes within the film.

In a third study of epitaxy mechanisms, LiNbO₃ (precursor: hybrid alkoxide) was grown on basal plane Al₂O₃ substrates (3). Both have similar structures with Li and Nb systematically replacing Al. The large lattice mismatch (~8%) appears to be responsible for the "mosaic" character of the film and a second epitaxy orientation described by an in-plane rotation of 60°. Mosaic character describes a film composed of small regions that are slightly rotated relative to one another and the substrate (up to 5% in this case) (3). Mosaic regions are undesirable because their boundaries scatter light, and the grooves formed where the boundaries intersect the surface produces a "rough" surface which also scatters light. Films grown by vapor routes have similar defects. A Fe₂O₃ epitaxial buffer layer (produced with a Fe-hexanoate precursor) between the Al₂O₃ substrate and LiNbO₃ film, which reduces the lattice mismatch to 2%, lowers the mosaic character and eliminates the in-plane, 60° rotation variant (3).

When the mismatch strain exceeds ~8%, the epitaxy phenomena is not the grain-growth phenomenon described above, but appears to occur by concurrent abnormal growth and an instability phenomena described below.

Epitaxy During a Phase Transformation

In another study (5), a hybrid-alkoxide (AcPbOTi(OR)₃) precursor was used to form epitaxial PbTiO₃ thin films on cubic (100) SrTiO₃ substrates. After heating to ~400°C for 1 hour, a polycrystalline, metastable pyrochlore phase crystallized from the pyrolyzed amorphous precursor. At

~420°C for 1 hour, the thermodynamically stable phase, with a perovskite structure, epitaxially nucleated at the film/substrate interface. Only a few epitaxial grains per unit area "burst" through the film toward the surface over a small temperature range to consume all of the nanocrystalline fluoride grains and trap the nanopores that were in the pyrolyzed film. These large, epitaxial grains are porous and exhibit a extensive mosaic character. Further heating densifies the perovskite grains and reduces their mosaic character. Pores, which coarsen with grain growth, produce a pitted surface as they disappear from within the film. At 800°C for 1 hour, a dense epitaxial PbTiO₃ film with a smooth surface is produced (Fig. 7). Figure 7 also shows that the film contains twins, caused by its cubic to tetragonal structural transformation during cooling through its Curie temperature (~480°C). Laths of a axis domains in a c axis film help relieve strain energy that arises during the structural transformation.

In the PbTiO₃ study (5), the initial polycrystalline film did not have the same structure as the substrate, and the driving force for the nucleation and growth of the epitaxial grains was different relative to the epitaxy of Zr(Y)O₂ on Zr(Y)O₂ (11). In systems that directly crystallize to the stable structure, elimination of grain boundary area per unit volume is the only decrease in free energy driving epitaxial grain growth. In the case of the PbTiO₃ epitaxy, the metastable pyrochlore to perovskite transformation provides an additional decrease in free energy. It appeared that this extra driving potential not only allows only a few large grains to rapidly grow through the polycrystalline film but also leads to entrapped porosity and the less ordered growth of the single-crystal thin film.

Abnormal Grain Growth and Morphological Instabilities

The most general case for epitaxy occurs when the film and substrate do not have the same structure. Once the width of the grains within a polycrystalline film is greater than the film thickness, grains with specific orientations will undergo abnormal grain growth because of their lower surface energies, or interfacial energies, or both (34). Thus, polycrystalline films with columnar microstructures are expected to undergo abnormal grain growth and to develop at least one preferred orientation even when the substrate is amorphous.

In addition to abnormal grain growth, the film can also undergo a morphological instability that causes it to uncover the substrate during grain growth. This phenomenon eventually produces a microstruc-

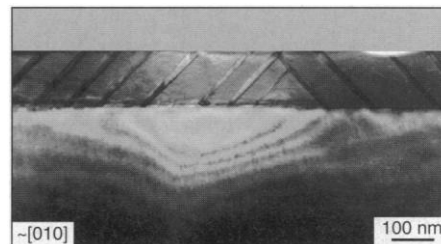


Fig. 7. Cross-sectional view of a tetragonal PbTiO₃ epitaxial film on a SrTiO₃ substrate. The film was heat-treated at 800°C, where the perovskite structure becomes cubic. Diagonal bands are 90° twins formed during cooling when the film transforms to its tetragonal, ferroelectric structure (5).

ture where every grain is an island. Srolovitz and Safran (35) were the first to predict this instability phenomena. They showed that a pin hole could grow in a polycrystalline thin film by deepening of the grain boundary grooves at a three-grain junction during grain growth. Miller *et al.* (36) confirmed this uncovering phenomenon with polycrystalline Zr(Y)O₂ thin films on sapphire substrates. They also presented a thermodynamic analysis showing that the breakup process lowers free energy of the system when the grain size (D) to film thickness (t) ratio exceeds a critical value, $(D/t)_c$, which depends on the dihedral angle (a measure of the grain boundary to surface energy ratio) and the solid-state "wetting angle" of the isolated grains on the substrate.

Miller *et al.* (36) summarized their thermodynamic calculations with an equilibrium, configurational diagram (Fig. 8), where D/t ratio is plotted as a function of the solid-state wetting angle for a specific value of the ratio of the surface to grain-boundary energies. One boundary in this diagram represents the condition (values of D/t and solid-state wetting angle) where free energy of the coherent film (represented by hexagonal, truncated grains) is equal to that of the film broken into isolated, single-crystal is-

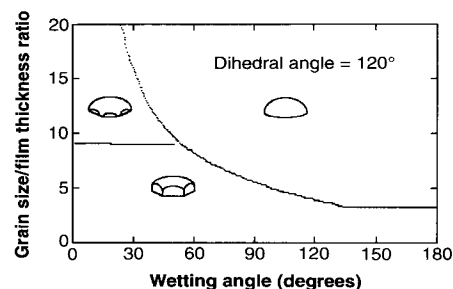


Fig. 8. Equilibrium configuration diagram for polycrystalline thin films with columnar microstructures. Boundaries represent the conditions (grain size/film thickness ratio and solid-state wetting angle) where different configurations have the same free energy (37).

lands (spherical caps). A third configuration also exists where grains are still joined by grain boundaries but the substrate is uncovered where three grains meet. As illustrated, the coherent film only exists over a small range of D/t . For very thin films, only a small amount of grain growth is required to cause the polycrystalline film to break up, uncover the substrate, and reduce free energy of the system.

For most film applications, the instability phenomenon is unwanted, but this breakup process can be used to produce "seeds" to grow a polyvariant crystal thin film (all grains have the same out-of-plane orientation) by recoating the substrate containing the oriented, isolated grains (the seeds) that are used to consume the much smaller grains within the new deposition through grain growth (37). This seeded growth method was recently used to eliminate the unwanted 60° variant for epitaxial LiNbO_3 films on an Al_2O_3 substrate (9).

A second type of morphological instability, which causes a single-crystal film to uncover the substrate, was recently discovered (38) when very thin, single-crystal PbTiO_3 films were grown on a SrTiO_3 . This instability phenomena is observed when the surface of a hole has a lower specific energy than the surface of the film. Experimental observations showed that three different film configurations may exist, which depend on the film thickness: thick films completely cover the substrate whereas preexisting holes in thinner films can grow to either form a continuous film containing an equilibrium area fraction of holes or they can grow together to cause the film to break up into single-crystal islands. A free energy model, which includes surface energy anisotropy and the spacing between preexisting holes, was used to explain this instability phenomenon (38), and showed that preexisting holes in thinner films will uncover the substrate. For the range of surface energies commonly observed in the inorganic materials of interest, preexisting holes

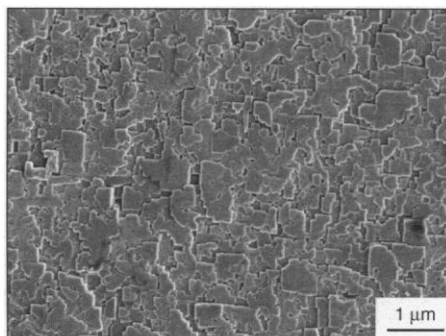


Fig. 9. PbTiO_3 epitaxial film synthesized directly from water at 150°C on a (100) SrTiO_3 single-crystal substrate (49).

greater than a critical size are necessary to initiate the instability.

Patterning

Many device applications, such as optical wave guides, require patterned thin films. After forming a precursor film produced with mixed metal carboxylates, such as hexanoates, Mantese *et al.* (20) have formed useful device patterns by only pyrolyzing the selected regions with a scanning laser. Unscanned areas can be simply washed away with the same solvent used to formulate the initial precursor solution. Yogo *et al.* (39) have applied photolithography techniques to form patterns by adding a photosensitive chemical (1-phenyl-1,3-butanedione), designed to have a specific ultraviolet absorption at 330 nm, to their mixed alkoxide precursor to form patterned single-crystal films of LiNbO_3 on sapphire substrates.

More recently, Jeon *et al.* (40) adopted the innovative method developed by Kumar and Whitesides (41) of stamping hydrophobic patterns on nearly any surface to produce patterned, epitaxial LiNbO_3 films on sapphire. This method uses a rubber stamp and an ink that renders the stamped surface hydrophobic. The rubber stamp is produced from a relief pattern formed on a Si substrate by conventional photolithography and etching techniques, and thus has the potential for submicrometer resolution. The inks are bifunctional molecules; one end reacts with the $-\text{M}-\text{OH}$ surface sites to chemically attach a hydrocarbon chain, which renders the surface it prints, hydrophobic. Jeon *et al.* (40) showed that spun-on precursor does not bond to the substrate at hydrophobic sites, and thus is easily removed after pyrolysis. With further development, this method appears to have the greatest potential to form the three-dimensional thin-film structure needed for advance device technology.

Epitaxy in Water

Hydrothermal methods have been used to synthesize ceramic powders (42) at elevated temperatures and pressures. Although hydrothermal generally denotes high temperatures and pressures, many binary, ternary, and more complex oxides are stable in water at ambient pressures and moderate temperatures. For example, thermodynamic calculations for the $\text{Ba-Ti-H}_2\text{O}$ system have been used to assess the relative stability of barium titanate in aqueous solution as a function of pH and reagent (Ba^{2+}) concentration. Thermodynamic calculations show that BaTiO_3 is favored at $\text{pH} > 12$ and high concentrations (2 M) of Ba^{2+} (43). For example, the BaTiO_3 can be directly synthesized from an aqueous solution as a powder (44, 45) and as poly-

crystalline thin films (46, 47). Lilley and Wusirika (44) patented the production of submicrometer BaTiO_3 powder using the hydrothermal method by reacting TiO_2 powder in a boiling, aqueous solution of barium hydroxide for ~ 48 hours. Others have used titanium sources such as Ti metal (46) and TiO_2 gels (45) at temperatures ranging from 100° to 400°C .

The hydrothermal, heteroepitaxial growth of BaTiO_3 was shown by Chien *et al.* (48) at 90°C by simply placing a SrTiO_3 single-crystal substrate into the beaker used to synthesize powder as described by Lilley and Wusirika (44). Chien *et al.* discovered that nanometer BaTiO_3 crystals nucleated at steps on the substrate surface and grew together to form the single-crystal film. Likewise, $\text{Pb}(\text{Zr}_x\text{Ti}_{1-x})\text{O}_3$ heteroepitaxial thin films were produced in an aqueous solution (10 M KOH) at ambient pressure and low temperatures (90° to 150°C) on (001) SrTiO_3 and LaAlO_3 single-crystal substrates (49). Growth of the $\text{Pb}(\text{Zr}_x\text{Ti}_{1-x})\text{O}_3$ thin films initiates by the formation of {100} faceted islands (49). Compositional analysis on the $\text{Pb}(\text{Zr}_x\text{Ti}_{1-x})\text{O}_3$ thin film shows that the Zr:Ti ratio is 44:56, nearly identical to the molar ratio of the precursors [TiO_2 powder, ZrOCl_2 , and $\text{Pb}(\text{NO}_3)_2$]. Figure 9 shows the faceted surface of a PbTiO_3 film epitaxied on a SrTiO_3 substrate. Epitaxial films of TiO_2 (50) and ZnO (51) on Si substrates have also been reported.

Although the thermodynamic stability of these and other important oxides are reasonably established, the details of their synthesis reactions and epitaxial growth mechanism are still unclear and the subject of current research.

REFERENCES AND NOTES

1. E. G. Bauer *et al.*, *J. Mater. Res.* **5**, 852 (1990).
2. D. P. Parlow and J. Gregg, *J. Mater. Res.* **2**, 595, (1987); S. Hirano and K. Kato, *Adv. Ceram. Mater.* **3**, 503 (1988); K. Nashimoto and M. J. Cima, *Mater. Lett.* **10**, 348 (1991); V. Joshi, G. K. Goo, M. L. McCartney, *Proc. Mater. Res. Soc. Symp.* **271**, 377 (1992); N. H. Hur, Y. K. Park, D. H. Won, K. No, *J. Mater. Res.* **9**, 980 (1994); K. Nashimoto, M. J. Cima, P. C. McIntyre, W. E. Rhine, *ibid.* **10**, 2564 (1995); N. L. Jeon, P. G. Clem, R. G. Nuzzo, D. A. Payne *ibid.*, p. 2996.
3. T. A. Derouin *et al.*, in press.
4. C. K. Barlingay and S. K. Dey, *Appl. Phys. Lett.* **61**, 1278 (1992); S. L. Swartz, S. D. Ramamurthi, J. R. Busch, V. E. Wood, *Mater. Res. Soc. Proc. Symp.* **243**, 533 (1992); S. Hirano *et al.*, *J. Am. Ceram. Soc.* **75**, 2785 (1992); B. A. Tuttle *et al.*, *ibid.* **76**, 1537 (1993); D. S. Yoon, C. J. Kim, J. S. Lee, W. J. Lee, K. No, *J. Mater. Res.* **9**, 420 (1994).
5. A. Seifert, F. F. Lange, J. Speck, *J. Mater. Res.* **10**, 680, (1995).
6. K. Vaidya, C. Y. Yang, M. de Graef, F. F. Lange, *ibid.* **9**, 410 (1994).
7. P. C. McIntyre, M. C. Cima, M. F. Ng, *J. Appl. Phys.* **68**, 4183 (1990).
8. S. J. Golden, F. F. Lange, D. R. Clarke, L. D. Chang, C. T. Necker, *Appl. Phys. Lett.* **61**, 22 (1992).
9. G. Braunstein, G. R. Pax-Pujalt, M. G. Mason, *J. Appl. Phys.* **73**, 961 (1993); S. Hirano *et al.*, *J. Am.*

- Ceram. Soc.* **76**, 1788 (1993).
10. K. T. Miller and F. F. Lange, *Proc. Mater. Res. Soc. Symp.* **155**, 191 (1989).
 11. K. T. Miller, C.-J. Chan, M. G. Cain, F. F. Lange, *J. Mater. Res.* **8**, 169 (1993).
 12. M. C. Cain and F. F. Lange, *ibid.* **9**, 674 (1994); K. T. Miller and F. F. Lange, *ibid.* **6**, 2387 (1991); A. Seifert, F. F. Lange, J. S. Speck, *J. Am. Ceram. Soc.* **76**, 443 (1993); P. K. Narwankar, J. S. Speck, F. F. Lange, *J. Mater. Res.* **10**, 1756 (1995).
 13. P. A. Langjahr, T. Wagner, M. Rühle, F. F. Lange, *Mater. Res. Soc. Symp. Proc.* **401**, 109 (1996).
 14. K. Okuwada, S.-I. Nakamura, M. Imai, K. Kakuno *Jpn. J. Appl. Phys.* **29**, 1153 (1990).
 15. D. Heimann, T. Wagner, J. Bill, F. Aldinger, F. F. Lange, in press.
 16. J. Livage, M. Henry, C. Sanchez, *Prog. Solid State Chem.* **18**, 259 (1988).
 17. C. J. Brinker and G. W. Scherer, *Sol-Gel Science* (Academic Press, New York, 1990).
 18. C. D. Chandler, C. Roger, M. J. Hampden-Smith, *Chem. Rev.* **93**, 1205 (1993).
 19. R. W. Vest, in *Ceramic Films and Coatings*, J. B. Wachtman and R. A. Haber, Eds. (Noyes, Park Ridge, NJ, 1993), pp. 303-341.
 20. J. V. Mantese, A. L. Micheli, A. H. Hamdi, R. W. Vest, *MRS Bull.* **14**, 48 (1989).
 21. E. Leroy, C. Robin-Brosse, T. P. Torre, in *Ultrastructure Processing of Ceramics, Glasses, and Composites*, L. L. Hench and D. R. Ulrich, Eds. (Wiley, New York, 1984), pp. 219-231.
 22. J. D. Birchall, *Trans. J. Br. Ceram. Soc.* **82**, 153 (1983).
 23. R. M. Laine and F. Babonneau, *Chem. Mater.* **5**, 260 (1993); J. Bill and F. Aldinger, *Adv. Mater.* **7**, 775 (1995); Y. Saito, S. Koyama, Y. Sugahara, K. Kuroda, *J. Ceram. Soc. Jpn.* **104**, 143 (1996).
 24. J. B. Blum and S. R. Gorkovich, *J. Mater. Sci.* **20**, 4479 (1985).
 25. A. D. Polli, F. F. Lange, C. G. Levi, unpublished work.
 26. A. D. Polli and F. F. Lange, *J. Am. Ceram. Soc.*, in press.
 27. D. E. Bornside, C. W. Macosko, L. E. Scriven, *J. Imaging Technol.* **13**, 122 (1987).
 28. A. G. Evans, M. D. Dory, M. S. Hu, *J. Mater. Res.* **3**, 1043 (1988); G. Gille, in *Current Topics in Materials Science*, E. Kaldis, Ed. (North-Holland, Amsterdam, 1985), vol. 12, chap. 7.
 29. J. W. Hutchinson and Z. Suo, in *Advances in Applied Mechanics*, J. W. Hutchinson and T. Y. Wu, Eds. (Academic Press, New York, 1991), pp. 63-191.
 30. D. K. Leung, C. J. Chang, M. Rühle, F. F. Lange, *J. Am. Ceram. Soc.* **74**, 2786 (1991).
 31. M. L. Balmer, F. F. Lange, C. G. Levi, *ibid.* **75**, 946 (1992).
 32. A. P. Sutton and R. W. Balluffi, *Interfaces in Crystalline Materials* (Clarendon, Oxford, 1995), pp. 129-131.
 33. P. A. Langjahr, T. Wagner, M. Rühle, F. F. Lange, unpublished results.
 34. C. V. Thompson, *Annu. Rev. Mater. Sci.* **20**, 245 (1990); _____, J. Floro, H. I. Smith, *J. Appl. Phys.* **67**, 4099 (1990).
 35. D. J. Srolovitz and S. A. Safran, *J. Appl. Phys.* **60**, 247 (1986).
 36. K. T. Miller, F. F. Lange, D. B. Marshall, *J. Mater. Res.* **5**, 151 (1990).
 37. K. T. Miller and F. F. Lange, *ibid.* **6**, 2387 (1991).
 38. A. Seifert, A. Vojta, J. S. Speck, F. F. Lange, *ibid.*, in press.
 39. T. Yogo, Y. Takeichi, K. Kikuta, S.-I. Hirano, *J. Am. Ceram. Soc.* **78**, 1649 (1995).
 40. N. L. Jeon, P. G. Clem, R. G. Nuzzo, D. A. Payne, *J. Mater. Res.* **10**, 2996 (1995).
 41. A. Kumar and G. M. Whitesides, *Appl. Phys. Lett.* **63**, 2002 (1993).
 42. W. J. Dawson, *Am. Ceram. Soc. Bull.* **67**, 1673 (1988).
 43. K. Osseo-Asare, F. J. Arriagada, J. H. Adair, *Ceramic Transactions*, G. L. Messing, E. R. Fuller, Jr., H. Hausner, Eds. (American Ceramic Society, Westerville, OH, 1988), pp. 47-53.
 44. E. Lilley and R. R. Wusirikka, U.S. Patent 4 764 493 (1988).
 45. D. Henning and S. Schreinemacher, *J. Eur. Ceram. Soc.* **9**, 41 (1992).
 46. Y. M. Yoshimura, S. E. Yoo, M. Hayashi, N. Ishizawa *Jpn. J. Appl. Phys.* **28**, 2007 (1989).
 47. E. B. Slamovich and I. A. Aksay, *J. Am. Ceram. Soc.* **79**, 239 (1996).
 48. A. T. Chien, J. S. Speck, F. F. Lange, A. C. Daykin, C. G. Levi *J. Mater. Res.* **10**, 1784 (1995).
 49. A. T. Chien, J. S. Speck, F. F. Lange, unpublished results.
 50. Q. Chen *et al.*, *Appl. Phys. Lett.* **66**, 1608 (1995).
 51. Q. Chen, Y. Qian, Z. Chen, Y. Zhang, *Mater. Lett.* **22**, 93 (1995).
 52. This review was supported by the Air Force Office of Scientific Research under grant F49620-93-1-0358DEF. Research concerning hydrothermal epitaxy was supported by the National Science Foundation to the UCSB/Materials Research Laboratory under the award, DMR-9123048.

Device Applications of Side-Chain Ferroelectric Liquid Crystalline Polymer Films

K. M. Blackwood

Side-chain ferroelectric liquid crystalline polymers are currently used in a number of applications, including displays and electrical sensors. Comparisons with existing technologies and materials indicate that relative to ceramics, such polymers have lower figures of merit but offer greater durability in sensor applications.

Side-chain liquid crystalline polymers (SCLCPs) may be thought of as having normal polymeric backbone architectures with pendant groups that show LC properties. In 1978, Ringsdorf and co-workers conducted systematic studies of SCLCPs (1, 2) and showed that, in order to preserve the LC phase behavior of the mesogen, it was necessary to insert a flexible spacer between the main chain and the core. Schematically the structure of a SCLCP can be represented as in Fig. 1.

The response time of a ferroelectric LC material can generally be related to its viscosity as

$$\tau \approx \eta / (EP_s) \quad (1)$$

where τ is the response time (the response time of a LC device is typically taken to be the time required for a 90% change in the amount of light transmitted through the device), E is the applied field, P_s is the spontaneous polarization of the sample, and η is the bulk viscosity. In a polymer that, even above its glass transition temperature T_g , is more of a viscoelastic solid, the response time will be exceptionally slow in comparison with traditional LC materials. Given this, one may wonder what drives the study of SCLCPs other than mere academic interest. The answer arises from developments in the low molecular weight area. In 1974, Meyer *et al.* showed mathematically that, if one could unwind the helical su-

perstructure of a chiral smectic C-phase LC, then the low degree of symmetry would lead to the development of ferroelectricity (3). This phenomenon can be understood by considering the arrangement of the mesogens within the smectic C phase. LC materials can exhibit many phase structures between the isotropic melt and the solid crystal. Of these mesophases, the best known is the nematic phase, in which the mesogenic units have a degree of long-range ordering not present in the isotropic melt. This ordering causes the rod-like mesogens to adopt a preferred orientation. This preferred orientation is known as the director, and the movement of this director by electric fields (Fig. 2) is the basis for the present generation of LC displays.

In their quest for better, faster displays, researchers turned their attention to the smectic mesophases. Here, the mesogens arrange themselves into distinctive layers, although there is little positional ordering

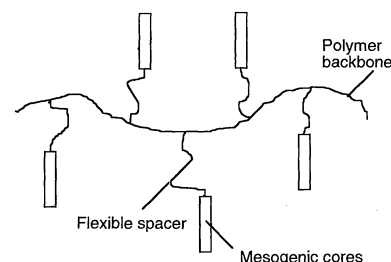


Fig. 1. Schematic diagram of SCLCP architecture.

The author is with the Defence Research Agency, St. Andrews Road, Great Malvern, Worcestershire WR14 3PS, UK.